Journal of Engg. Research Vol. 7 No. (2) June 2019 pp. 89-104

Introductory review of potential applications of nanoseismic monitoring in seismic energy characterization

Yawar Hussain*, Hernan Martinez-Carvajal*, Martin Cárdenas-Soto** and Salvatore Martino***

**Department of Civil and Environmental Engineering, University of Brasilia, Brazil*
***Engineering Faculty, National Autonomous University of Mexico, Mexico City, Mexico*
****Department of Earth Sciences and Research Center on Geological Risks, University of Rome "Sapienza", Italy*
**Corresponding Author: yawar.pgn@gmail.com*

ABSTRACT

Major terrestrial hazards are associated with the formation of fractures that evolve with time and lead to structural collapse. The fracture signals emitted in response to stress accumulation and its release, if properly understood, provide sound background for the development of Early Warning Systems (EWSs). Different attempts have been made in the past for their proper understanding, but in this study Nanoseismic Monitoring (NM) is being discussed, in terms of its sensor employment and signal processing modules. NM is a method dedicated to the detection, localization, and characterization of very low-energy seismic signals (M_L<1) at short distances (<10 km). Data are acquired by small aperture (max 200m) seismic arrays that are easy to install and consist of one central three component (3C) sensor surrounded by three vertical one-component (1C) sensors in a tripartite layout that are suited for the beam forming processing. Detection and location of weak events are done by dedicated software: the NanoseismicSuite, which was developed at Stuttgart University, Germany. The signals are processed by sonograms (*i.e.,* spectrograms with a frequency-dependent noise adaptation). The sonograms enhance the display of weak signal energy down to the noise threshold and allow supervised pattern recognition of weak target events in the frequency domain. Locations of weak events are supported by a graphical jackknifing approach. The case studies have shown that NM can successfully detect various weak fracture signals induced by the (stress relief mechanisms of near-surface geoprocesses) landslide dynamics, structural health, hydraulic fracturing, erosional features, pre-mature sinkholes, pending rock fall, and micro-seismicity associated with active faults.

Keywords: early warning systems; fracture signals; mini-array; slidequakes; sonograms.

INTRODUCTION

Materials under stress emit specific signals before their final collapse. These fracture signals/stress relief mechanism having low energy usually lesser than zero at local magnitude scale (M_L) (Walter et al., 2011). The magnitude is a number that characterizes the relative size of an earthquake. Several scales have been defined, but the most commonly used is local magnitude (M_L). Micro-earthquakes in response to material instabilities cause micro-fractures usually referred to as quakes/slidequakes that grow with time and lead to complete failure (Gomberg et al., 1995). These low magnitude events (Ml< 0) could also be named "nano-earthquakes" (Butler, 2003; Häge & Joswig, 2008), which are impulsive in nature and vary in frequency, duration, and spectra and are attenuated at shorter slant distances, especially in unconsolidated materials like clays (Wust-Bloch & Tsesarsky, 2013). The information coded on these signals can be utilized for proper understanding of material unsuitability that lead to strengthen early warning systems (Sick et al., 2013). These signals are associated with major global hazards like soil erosion, structural heath, land sliding, and sinkhole collapses. Each one has its own share in the total annual global hazards (Planes et al., 2016). The effects of these hazardous phenomena can be mitigated by strengthening Early Warning Systems (EWS) based on better detection and localization of these signals.

Main challenge for the use of seismology at engineering scale is its low detection that limits the understanding of onset and propagation of seismic signals through materials, mainly low magnitude and low signal to noise ratio (SNR), particularly in urban areas. These shortcomings in the traditional seismology gave rise to new techniques for the better understanding of weak seismic signals at smaller scales, with their own merits and demerits. The situations where low energy and high frequency signals emitted from the source at smaller distances from receivers, the phase picking, and source location by seismographs fail. In these situations various techniques have been proposed like beam forming, polarization, and Hypolines.

Microseismic monitoring (MM) is the measurement of small earthquakes, not detectable by humans, mostly by the induced material deformation. In MM events are located by the Geiger approach where correct event localization is based on correct onset (Häge & Joswig, 2008). The passive seismic monitoring offered new improvement, sequence of events is located based on the concentration of recorded energies, and the individual events cannot be separated (Häge & Joswig. 2008). Joswig (2008) introduced Nanoseismic Monitoring (NM) that fill the gap between microseismic and passive seismic monitoring. It took the seismic monitoring to new highs by increasing its sensitivity down to noise levels. The new demands for the sensitivity in fracture signal detection, characterization and localization, were achieved by the specialized deployment of sensors (min-array) and advanced signal processing with dedicated NanoseismicSuite software (Sick et al., 2014).

NM has been applied to many studies until now since its first application to identify sinkholes before their collapse in Israel; a (Wust-Bloch&Joswig,2006). A similar technique was applied to Heumoes landslide in Austria. (Walteretal., 2011). That slope was creeping in nature, which had been resolved into discrete rupture episodes on the basis of seismic rupture signals. NM was applied for the detection of small noisy or impact signals to Super-Sauze mudslide in the southern French Alps, where waveform and sonogram analysis were applied to discriminate the event types and on the basis of the spatial distribution of their epicenters the authors notified a mechanical phenomenon associated with each type of signal. From that study, it was concluded that the slide obviously relieves stress continuously, but extensive rainfall can trigger stronger material failure processes. (Walter & Joswig, 2009). Another study was conducted at the Super-Sauze in which NM benefited from Unmanned Ariel Vehicle (UAV) (Walter et al., 2009). In the Austria and Alps cases, processes were constrained by the uppermost meter where mudslide material dries out in summer to consolidate with sufficient shear resistance (Walter et al., 2013). In Israel, a study was conducted that demonstrated the potential of NM in rapidly detecting, locating, and analyzing brittle failure generated within unconsolidated material before the occurrence of total collapse.(Wust-Bloch,2009). The countrywide adaptability of NM has made it an attractive choice for the experts from various fields of earth sciences and engineering.

The present paper is an attempt to provide, a brief methodological introduction to NM along with its potential applications in the historical context. The countrywide applicability as well as introduction of dedicated NanoseismicSuite software package is also taken under consideration. This article will help the readers to have a quick overview of the working principle, application history, and some limitations of NM.

NANOSEISMIC MONITORING

NM is a field of passive seismic, constituting of specialized acquisition and processing methods for the detection and localization of weak energy signals (M_L<1) usually less than background noise levels (Wust-Bloch and Joswig, 2006; Wust-Bloch, 2009; Walter et al., 2011; Wust-Bloch and Tsesarsky, 2013; Joswig, 1990; 1995). The robustness against noise levels and autonomy in event detection are the two aspects of this technique that took it to new highs of unprecedented sensitivity. The essence of autonomy lies in the application of Seismic Navigation System (SNS) because it can be achieved on the principle that event of weak magnitude can be detected at nearest station only. And the second pillar of NM, i.e., robustness against noise is achieved in signal processing where detected software 'HypoLine' reduces the signal detection below zero decibel (db). The rapid system setup, together with its ultra-portability, turns the SNS into a truly optimal aftershock monitoring system (Joswig, 2008).

Mini-array

The use of sensors arrays can be traced back to 1960s. In comparison to single station array has many advantages that are useful in engineering applications. The name SNS will differentiate it from single station on the other hand from microseimic network (Joswig, 2006). Each mini-array consists of one three-component and three vertical one-component seismometers installed at an appropriate angle (120^0) (**Fig. 1**). The aperture size is a function of slant distance (source-receiver distance), which is usually kept in the range of 50-200m (Joswig, 2008). The aperture is a very crucial component of this system because it will resolve only those events that lie within this array aperture. Because the target signals in NM are characterized by high frequency contents, the choice of the sensors is usually short period seismometers both one component and three components together with high sampling rate and continuous data loggers.

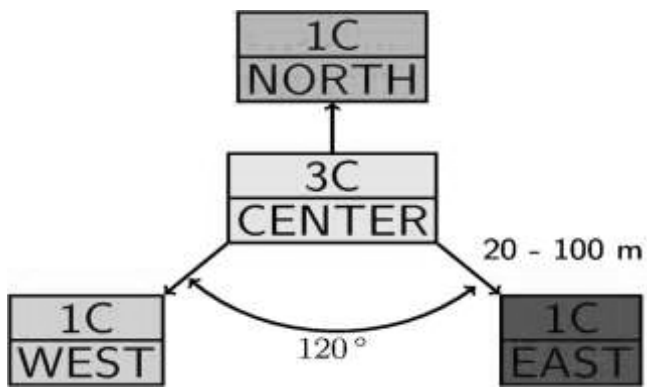

Fig. 1. Data acquisition with SNS (Sick et al., 2014).

The importance of seismic arrays in the detection of events cannot be neglected from local to teleseismic scales. Their operations are similar to phased arrays used in radar acquisition and were applied first time to seismic problem in the 1960s (Rost & Thomas, 2002). The maximum phase coherence among all stations is achieved by utilization of the concept that plane waves travel along the array aperture. Then the SNR is improved by utilizing the sum and delay concepts commonly referred to as beam forming, where SNR is taken proportional to the square root of number of stations used. In turn array gives only one location by using many stations. The three-component stations provide the back azimuths from station to event and are constrained in the direction of tS-tP (time difference between S and P waves) that provide distance in this way; the events are localized (Joswig, 2008).

Data processing

In absence of a priori velocity model the signal processing in NM is of constant loop type, which rests on trial and error approach. Both array and network analyses were introduced to see the influence of single trace in the location space. The signal energy is displayed in time-frequency domain and slowness space. The error bars are accessed by jackknifing trough hundreds of options in parameter space in a virtual reality manner. In NM the nano-events having M_L -2.0 are obtained from cross-correlation of captured earthquake events of M_L 0.0 (Joswig & Schulte-Thesis, 1993). Data processing in NM has following important steps. Data is processed using a software package named NanoseismicSuite (Sick et al., 2014).

Sonograms and Supersonograms

The sonogram is a graph, where the vertical axis is the logarithm of the frequency and the horizontal axis is the time. This graph allows the user to view the energy density as a function of time-frequency (Joswig, 1990). The sonogram calculation is carried out through the following four steps: 1) Power Spectral Density Matrix (PDM); 2) the energy binned at 13 half octave wide bandpasses and results are being transformed to a logarithmic scale; 3) in this

step a noise adaptation by Stive filter is applied, with the advantage of applying this filter being that it rates the fracture action of energy, which differentiates it from background noise; 4) the last step is the prewhitening, the objective to mute the analogues noise spikes in order to avoid disturbances in signal visualization (Joswig, 1990; 1995; Sick et al., 2014; Vouillamoz, 2015). A typical sonogram is shown in **Figure 2**. The spectral whitening equalizes the spectrum of the signal by enhancing low level spectral components and attenuating high level ones, making it similar to the white noise spectrum (spectral amplitude equal to one). Here the aim is to remove the influence of signals, which manifest in amplitude spectra such as frequency-localized noise sources. Thus, knowing the characteristic spectral content of some types of noise or events of interest, we can identify them (Joswig, 2006).

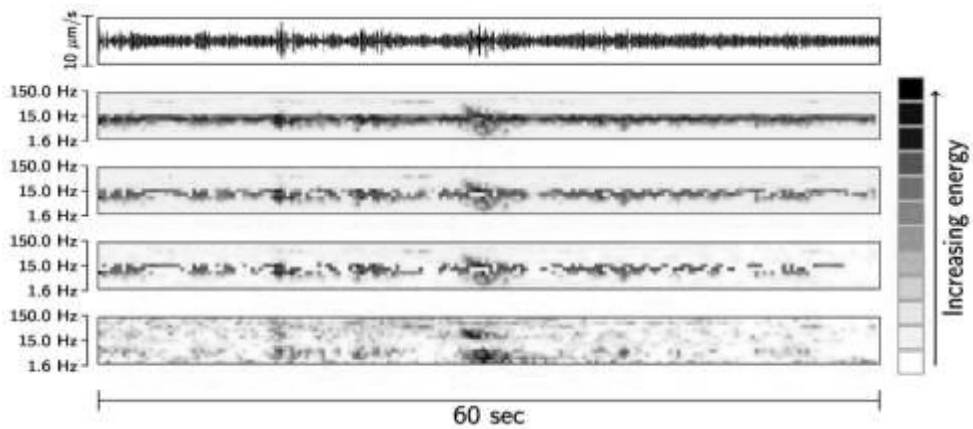

Fig. 2. An example of Sonogram (Sick et al., 2014).

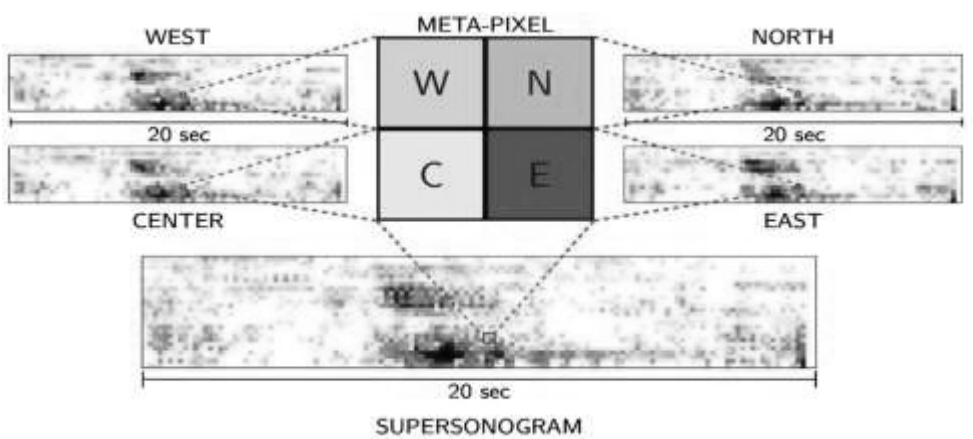

Fig. 3. A presentation of supersonogram (Sick et al., 2014).

Hypoline and jackknifing

Here the contribution of each individual phase in event location is displayed as hypolines (constraining curves in event location or hyperbola of tp-tp at any two stations or circles of ts-tp of any single station; it can be an array beam) and is determined by HypoLine program. The highest concentration of these hypolines in solution space is the best event location. These hyperbolae are best suited for half space solution models and with zero depth. The increase in depth will leave a cut on the surface (hyperboloid), which becomes hyperbola when this cut (hyperboloid) becomes parallel to the axis of symmetry. The ability of Hypoline in event localization depends on the handling and displaying the uncertainties. Like other classical approaches it also considers area of hypolines crossing like classical approach (matrix inversion), but unlike classical approach its values are determined by jackknifing (Joswig, 2006).

For the location of discrete events, the hypocenter related information is broken down into small graphical location constraints, which help in location of small events in a joint, average erroneous space. This form of outliers-resistant statics is referred to as Jackknifing and it has central role in the identification of nano events (Joswig, 2008). This scheme is a variation of the most common, "leave one out" jackknife where N observations are subdivided into N samples of size N-1, and, e.g., to train artificial neural networks on limited observation data. Here we perform a "leave out k" operation with N-k being the dimension of the statistics, i.e., matching the number of parameters to be determined (**Table 2**) (Joswig, 2006; 2008).

The iterative nature of HypoLine, which is present in SonoSuite, allowed a real time monitoring. The change in the obtained results like hypocenter, time of origin of the event, and magnitude can be done with simple clicks. The same iterative scheme can be applied to intrinsic parameters, such as velocities and thicknesses of the layers or magnitude-distance correction. The purpose of this interactivity is to test the possible combinations among the different phases for the same event, due to the low SNR, with the intrinsic parameters for the solution and arrives at a plausible solution (Joswig, 2008).

NanoseismicSuite

There are two main modules, HypoLine and Sonoview, of the NanoseismicSuite software (www.nanoseismic.net), developed by the Institute of Geophysics of the Stuttgart University. SonoView helps in screening the recorded data by the super-sonogram operator, i.e. a specific spectrogram with noise adaptation, muting and pre-whitening function and a special color palette that facilitates visual detection of seismic events (Sick et al., 2015).

It is a Java based user interface that provides the environment for carrying out all the processing steps of the NM. SonoSuite (software) package was developed by Joswig (2008). This software uses a graphical approach. Phases are determined interactively, and the results are updated in real time in the solution space. Locations are computed with a combination of arrays and networks processing with the following information: P arrival times, t_s–t_p time differences from the two central 3c's as well as array beams from the two mini-arrays. P and S onsets are determined interactively. Event detection is carried out with sonograms (Joswig 1990, 1995), which enhance the display of signal energy close to the noise threshold by auto-adaptive, non-linear filtering.

Signal nomenclature

The frequency contents, duration, and amplitude are the three basic attributes on which entire nomenclature of nano-signals is based. The attenuation characteristics of the site that affect these attributes have an important role in signal classifications (Walter et al., 2012).

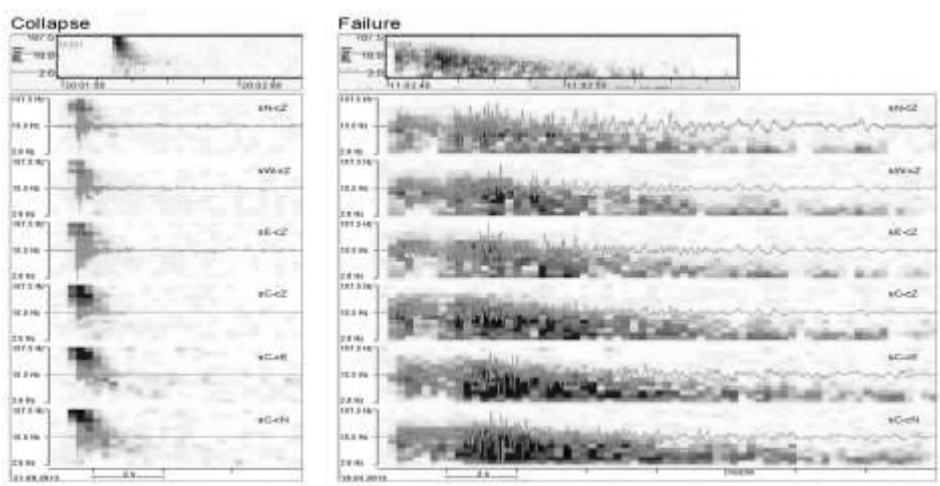

Fig. 4. Sonogram with waveform of collapse and failure events (Fiorucci et al., 2017).

Event Location

Events are localized in HypoLine by network and array processing (Joswig, 2006). In array processing backazimuth is calculated while in network t S -t P spheres and t P-t P hyperboloids of mini-array are determined where the accuracy of event location is dependent on the number of stations used and it can be optimized using hyperboloids of three small arrays (Häge & Jowsig, 2009). Event localization can be explained as an absolute location of homogeneous half space and a relative event as described below.

Absolute location

This event localization can be exemplified by considering a homogeneous half space below the surface where the sensors lie. The required information is derived from the time difference (tp1-tp2) of the P wave arrivals at two different sensors; the result is a semi-hyperboloid, which is converted to a hyperbola on intersection with a plane parallel to the surface at depth as shown in **Fig. 5a**. Imagine a seismic source S and two sensors S1 and S2 on the surface of earth. If t1 is the time taken by the wave emitted at S to reach at sensor S1 and t2 is the time taken by the wave from S2 to reach the second sensor S2, then the distance between the two sources can be determined by Equation (1). In Equation (1) an infinite combination of FS1 and FS2 is used, which results in the constant Δt. v (v is the propagation velocity of the wave). Equation (1) is a mathematical presentation of a case where two receivers lie at the foci of hyperbolae as shown in **Fig. 5b**.

$$F1S1 - FS2 = \Delta t.v \qquad (1)$$

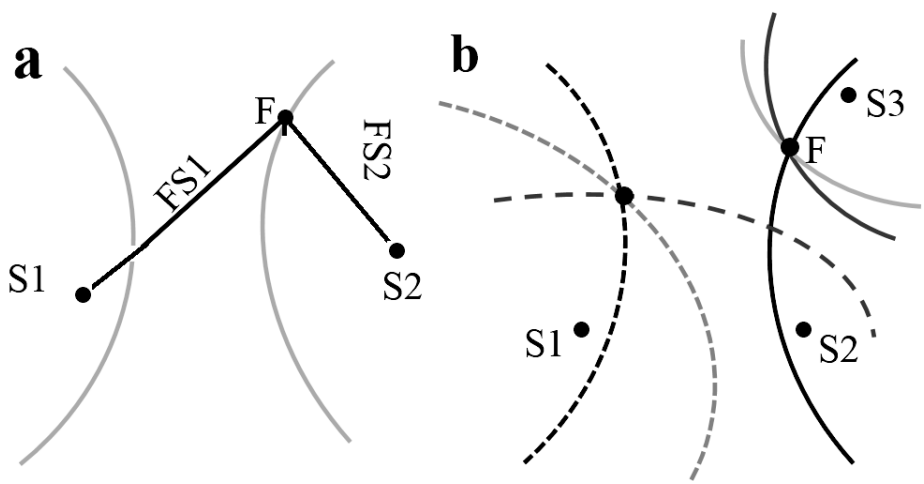

Fig.5. (a) Hyperbolae with two sensors at the foci and a signal solution (source location). (b) Intersection of three hyperbolae obtained from the distance of source and sensors. Dotted lines are the initial and solid lines are the final solutions, respectively (Modified after Silva, 2010).

Three sensors S1, S2, and S3 are shown for the source lactation. Their hyperbolae intersect twice, which is represented as dotted and solid lines as initial and final solutions, respectively (**Fig. 5b**). The arrival times of P-waves decide the fate of hyperbolae for the solution (contentious lines or dotted lines). Then, for a solution in space 3-D (x, y, z), x and y are the epicenters and z is the hypocenter, with only two receivers, which leads to more unknowns and the result will be underdetermined system (**Fig. 5a)**. The hyperbolae intersection points are determined by the difference in distance between source and receiver. At the beginning there are two points of intersections (dotted lines) but later depending on the time sequence in which waves strike the receivers there will be a single intersection (solid lines). Hence it is proofed that we need at least three receivers that all intersect at a single point, which is called as triple point and it is the solution.

Now let us consider a case where we have four sensors for the acquisition; here four intersection points are found P1= f(t1, t2, t3), P2 = f(t 1, t 2, t 4), P3 = f(t1, t2 , t4), and P4 = f(t2, t3, t4). There are four respective solutions in this case. Four triple points are visualized in HypoLine that creates a spread based on the phases then the hypocenter is localized.

$$P = f(t1, t2, t3) \tag{2}$$

Hyperboloids are calculated by tP –tP of different stations, whereby t1, t2, and t3 are P onsets at S1, S2, and S3, respectively. For instance, hyperboloid t13 for stations S1 and S3 is calculated by t13 = t1 –t3 (Häge & Jowsig 2009). Generally, the number of hyperbolae H is given by Equation (3), where N is the number of sensors and k is an integer ranging from 1 to N-1. The number of triple points T (solutions) is given by Equation (4). **Table 1** shows the triple point numbers (T) and (H) as a function of the number of sensors (N) used (Joswig, 2008).

$$H = \sum_{K=1}^{N-1} K = \frac{N!}{(N-2)!\,2!} \tag{3}$$

$$T = \sum_{K=1}^{N-2} K(N-1-k) = \frac{N!}{(N-3)!\,3!} \tag{4}$$

Table 1. Number of hyperbolae and triple points as a function of the number of receivers (Joswig, 2008).

N	3	4	5	6	7	8	9	10	11	12
H	3	6	10	15	21	28	36	45	55	66
T	1	4	10	20	35	56	81	120	165	220

Angle of incident of the wave with sensor is another information obtained from the analysis. In HypoLine this can be obtained either by triaxial receiver or by beam forming analysis (Joswig, 2006). In the first case, the vector information is derived by the wave recoded at three directions. The second method is based on the time difference of the same wave recorded at two receivers. Consider a plane wave front in two dimensions where t1 and t2 are the times when this wave reaches sensors S1 and S2, respectively. The distance of wave front is v.Δt, where Δt = t2 – t1. The propagation velocity is equal to true velocity only in the direction where sensors align **(Fig. 6b)**; in all other directions its value is smaller (apparent velocity) as shown in **Fig. 6.b**. This particular direction is the direction of event. As the distance between sensors is small (max. 100m) in NM, the waves emitted are considered as flat (**Figure 6**). This assumption is used in beam forming method. In the case where wave front is traveling in all directions the recorded velocity will be apparent velocity and is determined by Equation (5); it can also be written as Equation (6) in terms of slowness, where 'α' is the propagation velocity of the wave and 'i' the angle of incidence of the wave with sensor. In this way all the information required for the NM event analysis is obtained.

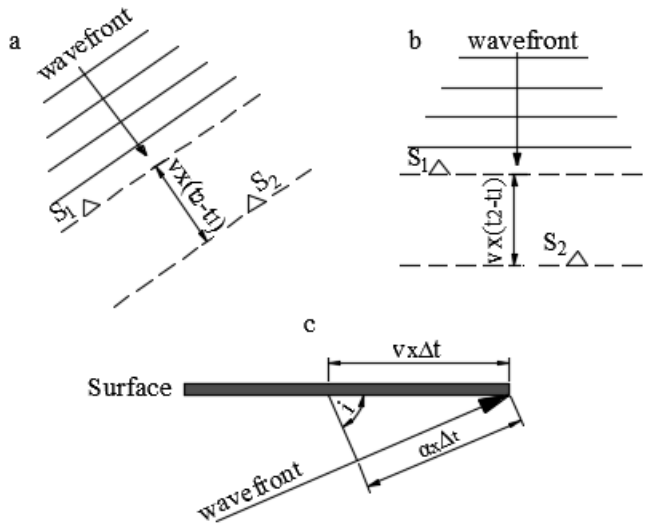

Fig.6. (a) Wave front incident on sensor S1 at time t1, after a time Δt = t2 -t1 on sensor S2 at angle. (b) Here wave front incident perpendicularly. **(c)** Velocity wave front α incident on the earth's surface at an angle i. (Lay & Wallace 1995).

$$v = \frac{\alpha}{sini} \quad (5)$$

$$v = \frac{1}{p} \quad (6)$$

Relative location

It is the location of an event from a main event with least location error. This works only if the distance between sensors is less than the distance of an event from sensor and events are so located have greater accuracy. Accuracy here depends on a situation where time residue at the middle is because of variation in propagation velocities of P and S waves. This time difference is calculated and then the locations of other events are corrected by using the obtained information manually by the observer in HypoLine. This relative location is obtained manually by the observer in HypoLine. This can be elaborated by considering a simple case where we have only three stations (**Fig. 7**); this simple approximation will facilitate understanding. The location obtained by intersection of tS–tP spheres and hyperboloids (tS–tP circles and hyperbolae in 2-D space) is considered as absolute. Green × marks the hypocenter. Using the location method (intersections of hyperbolae) for each pair of sensors (S*1-S2, S1-S3* and S*2-S3*), the difference of arrival time of the P wave of the secondary event, relative to the main event, is calculated by Equation (7).

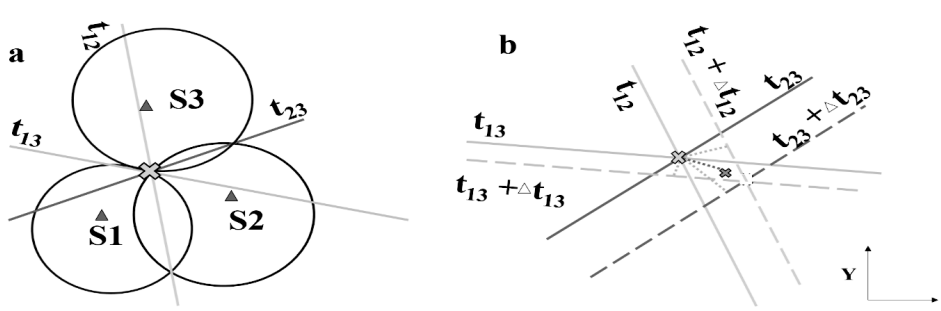

Fig. 7. Principle procedure of event location with network processing including data from three stations. Sketch in (a) shows the intersection of a horizontal plane at depth. Sketch in (b) is a zoom window of (a) (Häge & Joswig, 2009).

Fig. 7b shows an enlargement of Figure 8a, with the resulting dislocation vectors (continuous line of Red color) and the location of the event (red cross) in relation to the main event. The event secondary to the main event can be obtained by equation 7, which is equal to the sum of distance from the main event to the station with the distance from the secondary event to the main event.

$$\Delta tE12(relative) = \Delta tM12 + \Delta tM12 - \Delta tE12(absolute)$$

$$\Delta tE13(relative) = \Delta tM13 + \Delta tM13 - \Delta tE13(absolute)$$

$$\Delta tE23(relative) = \Delta tM23 + \Delta tM23 - \Delta tE23(absolute) \quad (7)$$

where 'E' and 'M' are the main and secondary events, respectively.

Magnitude

The magnitude of an event in NM is determined by the Wood-Anderson simulation (Häge & Joswig, 2009). The maximum and minimum amplitude values of the recorded waveforms can be determined easily. The magnitude values are shown as magnitude-distance correction curves and are calculated by Equation (8), where 'A' refers to the maximum amplitude, at the station site, and 'R' is the attenuation factor of the signal that travels from the source to the receiver. These magnitude distance corrections were proposed by Joswig (2006) and used in the Hypoline program.

$$M = log(A) + log(R) \quad (8)$$

APPLICATIONS

Applications of NM comprise aftershock surveys for natural and man-made seismic sources, active fault mapping, sinkhole activity, monitoring of volcanic and induced seismicity associated with LS, hydraulic fracturing, and engineering structures under stress (Joswig & Wust-Bloch, 2002; Wust-Bloch & Joswig, 2003).

Landslide monitoring

Evolutionary failure process leads to large scale deformation, which casts huge damage to lives, materials, and properties of the countries throughout the globe. It is very difficult to mitigate the effects of these hazardous because of non-linearity of multiple causing factors (Walter et al., 2011). This multiplicity stressed the need for the deployment geophysical instruments on these unstable slopes (Hussain et al., 2017). Different effectors have been carried out in the past for the analysis landslide dynamics. One of such effectors is NM, which was applied to Heumoes slope, Austria (Walter et al., 2011). This slope was creeping in nature and was resolved into discrete rupture episodes on the basis of seismic rupture signals. The spatial distribution of fractures was concentrated in those parts of the slope having higher deformational rates at the surface. The temporal occurrence correlated well with rainfall events and reinforced the assumption of a rainfall-triggered slope movement. The same technique was applied for the detection of impact signals at Super-Sauze mudslide in the southern French Alps, where waveform and sonogram analysis were applied to discriminate the variety of events and on the basis of the spatial distribution of their epicenters, a mechanical phenomenon was associated with each type of the signal. Authors concluded that the slide obviously relieves stress continuously, but extensive rainfall could trigger stronger material failure processes (Walter & Joswig, 2009).

However, monitoring results at two landslides, Huemose and Super-Sourse, in Europe showed the contradictory results. At one slope, the concentrations of slidequake/stress relief were maximum at the low displacement rates while at other these concentrations and displacement rates were aligned well. This problem was solved by Walter & Joswig, 2013, with NM; the authors concluded that these contradictory results were because of different relief topographies overlaying the bedrock. The bedrock influenced the stress mechanism.

In the case of Mudslide at Super Sauze, the events recorded by NM were divided into three categories based on the author's hypothesis. The first type of the signals was concentrated in portions of the slope that had maximum

movement; so these signals were linked to the fracturing in the moving mass. The second typology of events was populated near the free boundaries of the landslide mass, so it was were linked to scratching and grinding of the debris. Data acquisition consisted of 10 days recording with 4 SNS. Data was collected in continuous mode with sampling rate of 400. First the shorts were taken in order to determine the true velocity model. The data processing was done with HypoLine software as described above. The recorded material failure signals vary in duration, amplitude, frequency contents, and their sonogram patterns, based on these characteristics along with the site effects on the signals helping authors in signal nomenclature.

The precursory stress relief signals (-0.5 > Ml< 0.4) associated with rock mass failure were studied at Huemose slope some 5 km away from the Alps by using relative and master event localization approaches. Avalanche, as well as fracture signals, was observed with their relatively large epicenter distances. The meteorological factors were tested for the possible source mechanism detection but unfortunately, that was not resolved by the authors.

Table 2. F-t signatures and principal characteristics of seismic events induced by creeping LS dynamics (Vouillamoz, 2015).

Signal type	Time duration	Energy content & phases	Max.peak to peak amplitudes and local magnitudes	Source location	Numb. of recording seismometers	Number of events (weekly basis
Rockfall and avalanche (SS) Rock bearing faces	Few sec-20 min (single vs. multiple events)	High frequency noise band (up to 130 Hz): falling fine grained material Broadband spikes: falling blocks No phase identified	50-500 nm s-1: weak events recorded by a few stations only 500-1500 nm s-1: strong events recorded by complete network	Estimated by back azimuth	8-16	Up to 100's
Fracture (SS & HS) Rock bearing faces	≈ 2 sec	P phase: 50-100 Hz S phase: 10-70 Hz	≥ 1000 nm s-1 ML ≤ -0.5	Standard location procedure	4-20	1's – 10's
Slidequake (SS & HS) Within the LS body	SS: 2 – 5 sec HS: 0.5 – 4 sec	SS: P phase: 10-80 Hz Later phases: 5-30 Hz HS: P phase: 10-120 Hz Later phases: 10-70 Hz	40-2000 nm s-1 SS: -3.2 ≤ML ≤-1.3 HS: -2.2≤ ML ≤-0.7 Corresponds to fracture length of some meters	Standard location procedure SS: zone of highest displ. rate (11m y-1) directly linked to bedrock topography HS: zone of rel. lower displ. rate (0-5 cm y-1) directly linked to bedrock topography	4-12	SS: 10's Clustered HS: 1's Clustered
ETS-like Within the LS body	2-20 sec	≈150 Hz No phase identified	Just above noise level with enormous attenuation at higher recording distances	Estimation by back azimuth or closest recording station	4-8	10's-100's Clustered

Monitoring of gravity-induced slope deformations

NM was applied recently to a rock slope in noisy environment. The installation of SNS consisted of accelerometers and was divided into permanent and temporary networks. About 1300 events were detected with permanent SNS, then these events were divided into failures and collapse events based on their sonogram patterns (**Figure 4**). Then an index was developed based on the occurrence of these microseismic events and it would be used as a potential for alert. The recoded microseismic events were in good agreement with the evolutionary geological model of the ongoing gravitational slope deformation due to rock mass creep processes. Based on the potential use of NM authors had recognized collapse and failures related to inelastic rock mass deformations, and localization and magnitude calculation were done based on the physical parameters (frequency content, time duration, PGA, and AI) of the

recorded signals. The concentrations of so determined hypocenters were in agreement with the presence of gravity-induced slope deformations involving the rock masses (Fiorucci et al., 2016; 2017).

Structural health monitoring

Prefailure brittle impulsive signals emitted in response to applied stress were analyzed in three stages at Carverns in chalk. Wast-Bloch and Tsesarsky (2013) carried a study in which the waveform, associated with structural health, was characterized by Nanoseismic Monitoring. The study was carried out in three states: 1) complete characterization of signal in time frequency and space domains in a laboratory scale experiment. 2) These signals determined by NM were calibrated with the laboratory scale experiment result. 3) In the third and last stage the reliability of prefailure and failure signals were tested with the modelled stress distributions in the Carverns, which showed a good correlation with the concentration of microfractures determined by NM. The combined analysis was done with a marble plate subjected to four point bending tests. The impulsive signals associated with stress accumulation in marble plate (mm) were classified as Quake ($0.5 \geq t \geq 0.2$ s), Spike (< 0.05 s), Puff ($0.3 \geq t \geq 0.1$ s), and Tremor (> 0.3 s), based on full wave characterization. The events were linked to source processes by this controlled experiment setup. Results were compared with other techniques like acoustics. Beit Guvrin National Park (Israel) was then monitoring by a series of campaigns in order to understand the prefailure and post failure mechanisms in real field (natural) conditions. Four SNS were deployed to understand its prefailure dynamics by NM. Signal detection was done by comparing them with similar studies from the past and on site manual events simulations. The detected event magnitude ($-2.4 \geq Ml \geq -3.8$) was found similar to the signals emitted by the sandstone cliff (Wust-Bloch, 2010). Authors did not find sharp differences in the event duration of these sites.

Erosional cliff monitoring

Another important functionality of NM was observed in the seismic analyses of an unstable cliff at Mediterranean Sea. The erosion of banks by the accumulation of tidal energy is a continuous threat to structures and population at the sea shore. A dense network of SNS was deployed. The continuous six-hour recording gave the authors so many spiky nano-seismic signals associated with the cliff material deformation. Spatial distributions of maximum recorded amplitudes of nano signals gave rise to respective spatial distributions of deformational stresses in the cliff. Atypical event decay with time is because of post collapse stress accumulation that led to the appearance of tensile cracks (few cm) on the surface of cliff. This study has also strengthened the potential applicability of NM that had detected a well and identified the pre-collapse signals emitted by unstable cliff before total collapse with high confidence.

Pre-collapse identification of sinkholes

NM was first applied to identify sinkholes before their collapse in Israel (Wust-Bloch&Joswig, 2006). The low energy seismic events can be identified and located before total collapse with NM in unconsolidated layer media. Because of the absence of prior knowledge, authors performed many simulating experiments to calibrate their results. Waveform analysis was performed by sonogram, which categorized the signal into two events as impact in dry and impact on liquids. HypoLine (software) was successfully used to locate individual sinkhole events by just a few, low SNR seismograms, and M_L scale was calibrated to very low magnitudes, estimated from their source energy. It is now possible to monitor subsurface material failures before sinkhole collapse since the discrimination of impact signals based on their frequency content is indicative of the maturity of the cavitation processes.

Hydraulic fracturing

The fractures are created in the rock mass in response to pressurized fluids injection. This technique is being used to create permeable mass in the rock masses that increase the oil recovery by providing permeable mass for the fluid migration. These fractures generate microseismic signals. Location of these microseismic events is important in reservoir stimulation. Microseismic is a famous technique, which is used for analysis of hydraulic fractures, an expensive technique, and is also relaying on high SNR. Silva (2010) applied NM for the recording and localization

of microseismic events in response to injecting fluid. The events were separated by sonograms analysis and their localization was done by HypoLines. In that study field tests with controlled sources were performed at various distances from the sensors and were localized by NM. In a second test, perforation shots in a producing oilfield were monitored. One perforation shot was located with slant distances of 861 m and magnitude −2.4 M_L. Based on results the author reached a conclusion that the method has the potential to be used for monitoring hydraulic fracture.

Active fault mapping

The microseismicity associated with the active faults in Spain along with its relationship with regional catalog was studied for the very first time by Häge & Joswig (2009). Data was acquired with one SNS over the period of two nights at two different locations of Crevillente Fault Zone (CFZ). The magnitude threshold achieved during this campaign was M_L= -2.6. Gutenberg-Richter relationship was used to determine the occurrence of smaller events from larger earthquakes. However, this relationship was extrapolated by few researchers in order to determine larger events from smaller ones. The analysis of the frequency-magnitude distributions showed a good approximation among the amounts of recorded events with those of extracted from local catalogs.

Joint applications

The nonlinear interaction of multiple triggering factors has increased the vulnerability of models dealing with landslides because of the uncertainty involved in the determination of these parameters. In these conditions the single use of traditional models will produce erroneous results and joint analyses were suggested. Keeping this in mind the two high resolution techniques, NM and UAV based imaging of slope, were combined by Walter et al. (2009). The slope displacement analysis was done by comparing the stones, rocks, and vegetation present in the photographs taken at different times. At Super-Sauze the fracture and scratch signals were localized by the combined use of UAV and NM. In this campaign the resolution of 1-10 cm per pixels was achieved with flight height of 10-100 meters by a specially designed quad-rotor. This resolution per pixel is essential to identify the fractures. Some of the signals (34) were detected by clear onset phases on which the standard seismological processes were done. These detected signals have 2-3-second duration, frequency range is 10-80 Hz, and peak to peak amplitude value varies from 40 to 400 nm/s. Impulsive signals associated with brittle deformation were recorded by 10-day recording campaigns using SNS. The signals were then processed by Hypoline as described by Jowsig (2008). For the detection of these signals they must be recorded at least at two different stations. The estimated detection threshold for these events is M_L = -2.6 for a slant distance of about 140 m. The upper few meters surface of slope that was dried out in summers because of shear resistance was the home for the generation of both fractures and scratures. At Huemose slopes, which provide greater slope movements, a joint study was carried out by Walter et al. (2012). Here, the slide quakes generated in response to stress relief mechanism were analyzed and these events were mapped with combined use of NM reflection and refraction seismic. Authors concluded that the generations of slide quakes were related positively to the rain fall intensity. Nanoseismic findings were supported by the existence of fissure patterns at the slope surface, which could be observed by UAV-based remote sensing of the slope surface (Walter et al., 2009).

LIMITATIONS

Although NM is a new very promising technique, this technique has different limitations that should be considered before its implementation. In the case of the location of events, it is not possible to get an error associated with this location due to the fact that the procedure is based on a geometric formulation. This requires implementing a code that takes into account at least one model of small-scale velocities. The characterization of the seismic source is also required, that is, to obtain the tensor moment to determine the orientation of the fractures. Future studies will prove these assumptions.

The application of the technique of NM is also limited by the level of background noise. Special care must be taken when experiments are conducted in urban areas or when there is an intense industrial activity, as is the case of the mining areas (Fiorucci et al., 2016).

We believe that it is necessary to perform different experiments for different subsurface conditions, due to the fact that the environmental intrinsic attenuation can affect the results, in both the time domain and the frequency domain. For example, in the case of saturated clays with high coefficients of Poisson, the seismic signals are attenuated in high frequencies, and it would be difficult to obtain well-defined arrival times. Similarly, in media with high speeds it may be difficult to identify the phase differences between the primary and secondary arrivals.

CONCLUSIONS

This paper aims at providing a brief introduction of NM as a possible choice for the detection, characterization, and location of week seismic events having low energy usually associated with stress-relief mechanism. Following conclusions are being drawn by the authors.

To use the technique of NM it is necessary to perform a proper instrumentation according to the objective of the study. The different cases presented in this article show that the acquisition design, types of instruments, and the absolute control of the time are required to obtain excellent results.

In the experiments, it is necessary to take into account the characteristics of the environment. It is necessary to make a study of surface geophysics, geotechnical testing, and laboratory in order to improve the design of acquisition and the interpretation of the results.

Finally, this study shows that the technique of NM is a viable option for the detection, location, and characterization of seismic events of low energy associated with stress-relief mechanism.

ACKNOWLDGEMENT

The authors acknowledge the support of the following agencies: the National Council for Scientific and Technological Development (CNPq) and the Support Research of the Federal District Foundation (FAP-DF).

REFERENCES

Fiorucci, M. Iannucci, R. Lenti, L. Martino, S. Paciello, A. Prestininzi, A. & Rivellino, S. 2017. Nanoseismic monitoring of gravity-induced slope instabilities for the risk management of an aqueduct infrastructure in Central Apennines (Italy). Natural Hazards, **86**(2):1-18.

Fiorucci, M. Iannucci, R. Martino, S. & Paciello, A. 2016. Detection of nanoseismic Events related to slope instabilities in the Quarry District of Coreno Ausonio (Italy). Italian Journal of Engineering Geology and Environment, **16**(2).

Gomberg, J. P. Bodin, Savage, W. & Jackson, E. 1995. Landslide faults and tectonic faults, analogs: The Slumgullion earthflow, Colorado. Geology **23**(1):41–44.

Häge, M. & Joswig, M. 2008. Microseismic study using small arrays in the swarm area of Nový Kostel: Increased detectability during an inter-swarm period. Studia Geophysica et Geodaetica, **52**(4):651-660.

Häge, M. & Joswig, M. 2009. Microseismic feasibility study: detection of small magnitude events (ML< 0.0) for mapping active faults in the Betic Cordillera (Spain). Annals of Geophysics, **52**(2):117-126.

Hussain, Y., Soto, M. C., Carajal, H. M., Uagoda, R., Soares, J. & Martino, S. 2017. Spectral analysis of the recorded ambient vibration at a mass movement in Brasilia. Symposium on the Application of Geophysics to Engineering and Environmental Problems 2017: pp. 214-218. https://doi.org/10.4133/SAGEEP.30-012

Joswig, G. 1990. Pattern recognition for earthquake detection. Bulletin of the Seismological Society of America, **80**(1):170-186.

Joswig, G. 1995. Automatic classification of local earthquake data in the BUG small array. Geophysical Journal International, **120**(2):262-286.

Joswig, M. & G. H. Wust-Bloch 2002. Monitoring material failure in sinkholes in the Dead Sea area by four-partite small array

(Seismic Navigation System-SNS). Israel Geological Society, Annual Meeting, Maagen, Israel. p. 54.

Joswig, M. & H. Schulte-Theis, 1993. Master-event correlations of weak local earthquake by dynamic waveform match, Geophysical Journal International, **113**(3):562-574.

Joswig, M. 1993. Single-trace detection and array-wide coincidence association of local earthquakes and explosions. Computers and Geosciences, 19(2): 207–221.

Joswig, M. 1994. Knowledge-based seismogram processing by mental images. IEEE transactions on systems, man, and cybernetics, **24**(3):429–439.

Joswig, M. 2006. Nanoseismic monitoring: method and first applications, http://www.nanoseismic.net/

Joswig, M. 2008. Nanoseismic monitoring fills the gap between microseismic networks and passive seismic. First Break, **26**(6):117–124.

Joswig, M., Wust-Bloch, G. H. & Leonard, G. 2002. Nanoseismology: Development of an integrated technique for the monitoring of nanoseismic events triggered by natural subsurface material failure, Israel Atomic Energy Commission, Report # 2791458, 26p.

Lay, T. & Wallace, T. C. 1995. Modern Global Seismology. San Diego. Academic Press.

Planes, T. Mooney, M. A. Rittgers, J. B. Parekh, M. L. Behm, M. & Snieder, R. 2016. Time-lapse monitoring of internal erosion in earthen dams and levees using ambient seismic noise. Géotechnique, **66**(4):301-312.

Rost, S. & Thomas, C. 2002. Array seismology: Methods and applications. Reviews of geophysics, **40**(3).

Sick, B. Guggenmos, M. & Joswig, M. 2015. Chances and limits of single-station seismic event clustering by unsupervised pattern recognition. Geophysical Journal International, **201**(3):1801–1813.

Sick, B. Walter, M. & Joswig, M. 2013. Near-surface fracture and impact discovery from landslides and sinkholes by sonogram screening. First Break, **31**(8).

Sick, B., Walter, M. & Joswig, M. 2014. Visual event screening of continuous seismic data by supersonograms. Pure and Applied Geophysics,**171**(3-5):549-559.

Silva, A. G. D. 2010. Estudo do potencial da técnica de nanossísmica para o monitoramento de hidrofraturamento em reservatórios de hidrocarbonetos, Masters Thesis, Universidade Federal Do Rio Grande Do Norte, Natal, Brazil.

Vouillamoz, N. 2015. Microseismic characterization of Fribourg area (Switzerland) by Nanoseismic Monitoring, PhD Thesis, Institute of Geoscince, Stuttgart University, Stuttgart, Germany.

Vouillamoz, N. Wust-Bloch, G. H. Abednego, M. & Mosar, J. 2016. Optimizing event detection and location in low-seismicity zones: case study from Western Switzerland. Bulletin of the Seismological Society of America, **106**(5):2023–2036.

Walter M. Gomberg, J. Schulz, W. Bodin, P. & Joswig, M. 2013. Slidequake generation versus viscous creep at softrock-landslides: synopsis of three different scenarios at Slumgullion Landslide, Heumoes Slope, and Super-Sauze Mudslide. Journal of Environmental & Engineering Geophysics, **18**(4):269–280.

Walter, M. & Joswig, M. 2008. Seismic monitoring of fracture processes generated by a creeping landslide in the Vorarlberg Alps. First Break, **26**(6).

Walter, M. & Joswig, M. 2009. Seismic characterization of slope dynamics caused by softrock-landslides: The Super-Sauze case study. In Proceedings of the International Conference on Landslide Processes: from geomorphologic mapping to dynamic modelling: 215-220.

Walter, M. & Joswig, M. 2012. Seismic monitoring of precursory fracture signals from a destructive rockfall in the Vorarlberg Alps, Austria. Natural Hazards and Earth System Sciences, **12**(11):35-45.

Walter, M. Gomberg, J. Schulz, W. Bodin, P. & Joswig, M. 2013. Slidequake generation versus viscous creep at softrock-

landslides: synopsis of three different scenarios at Slumgullion landslide, Heumoes slope, and Super-Sauze mudslide. Journal of Environmental and Engineering Geophysics, **18**(4):269-280.

Walter, M. Niethammer, U. Rothmund, S. & Joswig, M. 2009. Joint analysis of the super-sauze (French Alps) mudslide by nanoseismic monitoring and UAV-based remote sensing. First Break, **27**:53–60.

Walter, M. Niethammer, U. Rothmund, S. & Joswig, M. 2009. Joint analysis of the Super-Sauze (French Alps) mudslide by nanoseismic monitoring and UAV-based remote sensing. First Break, 27(8).

Walter, M. Schwaderer, U. & Joswig, M. 2015. Analysis of pre-collapse failure signals from a destructive rockfall by Nanoseismic Monitoring. Engineering Geology for Society and Territory-Volume **2**:1531-1535.

Walter, M. Walser, M. & Joswig, M. 2011. Mapping rainfall-triggered slidequakes and seismic landslide-volume estimation at Heumoes slope. Vadose Zone Journal **10**(2): 487-495.

Wust-Bloch, G. H. & Joswig, M. 2003. Nanoseismic monitoring and analysis of extremely low-energy signals associated with subsurface material failures in unconsolidated layered media. ESG-EGU, Annual Meeting, Nice, France, Contribution EAEO3-A- 09794, Geophysical Research Abstracts, Vol. 5, 09794, 2003.

Wust-Bloch, G. H. & Joswig, M. 2006. Pre-collapse identification of sinkholes in unconsolidated media at Dead Sea area by "nanoseismic monitoring" (graphical jackknife location of weak sources by few, low-SNR records). Geophysical Journal International, **167**(3):1220-1232.

Wust-Bloch, G. H. & Tsesarsky, M. 2013. Structure health monitoring in natural environments: pre-failure event location and full-waveform characterization by Nanoseismic Monitoring. Journal of Environmental & Engineering Geophysics, **18**(4): 219–232.

Wust-Bloch, H. G. 2009. Characterizing and locating very weak ($-2.2 \geq Ml \geq -3.4$) induced seismicity in unstable sandstone cliffs by nanoseismic monitoring. Pure and applied geophysics, **167**(1-2):153-167.

Submitted: 01/01/2017
Revised: 02/02/2017
Accepted: 16/07/2017

مقدمة عن التطبيقات الممكنة لمراقبة النانو الزلزالي في توصيف الطاقة الزلزالية

ياور حسين، *هرنان مارتينيز كارواجال، **مارتن كارديناس-سوتو وسالفاتوري مارتينو**

*قسم الهندسة المدنية والبيئية، جامعة برازيليا، البرازيل

**كلية الهندسة، الجامعة الوطنية المستقلة في المكسيك، مكسيكو سيتي، المكسيك

***قسم علوم الأرض ومركز الأبحاث حول المخاطر الجيولوجية، جامعة روما "سابينزا"، إيطاليا

الخلاصة

ترتبط المخاطر الأرضية الرئيسية بتكوين كسور تتطور مع الوقت وتؤدي إلى انهيار هيكلي. إذا تم فهم إشارات الكسر الصادرة استجابة لتراكم الإجهاد وانبعاثه، بشكل صحيح، فإنها تصدر صوتاً على خلفية أنظمة الإنذار المبكر (EWS). وقد بُذلت محاولات مختلفة في الماضي لفهم تلك الإشارات على نحو سليم، لكننا نناقش في هذه الدراسة مراقبة النانو الزلزالي (NM)، من حيث عمل أجهزة الاستشعار ووحدات معالجة الإشارات. يُعرف الرصد النانو زلزالي بأنه الطريقة المُخصصة لاكتشاف وتوطين وتوصيف الإشارات الزلزالية منخفضة الطاقة (M_L<1) على مسافات قصيرة أقل من (<10km). يتم الحصول على البيانات من خلال مصفوفات زلزالية ذات فتحة صغيرة (بحد أقصى 200 متر) يسهل تركيبها وتتكون من مستشعر واحد مكون من ثلاثة مكونات (C3) محاط بثلاث مجسات رأسية أحادية المكون (C1) في مخطط ثلاثي ملائم لعملية تكوين الشعاع. يتم الكشف عن الأحداث الضعيفة وموقعها بواسطة برنامج مخصص: وهو برنامج النانو الزلزالي (NanoseismicSuite)، الذي تم تطويره في جامعة شتوتغارت، ألمانيا. وتتم معالجة الإشارات بواسطة أجهزة السونوغرام (أي، السبيكتوغرام المعتمد على التواتر المرتبط بتكيف الضوضاء). تعمل الإشارات الصوتية على تعزيز عرض طاقة الإشارة الضعيفة وصولاً إلى عتبة الضوضاء وتتيح التعرف على الأنماط الخاضعة للإشراف للأحداث المستهدفة الضعيفة في مجال التردد. يتم دعم مواقع الأحداث الضعيفة من خلال نهج jackknifing البيانية. أظهرت دراسات الحالة أن جهاز الرصد النانو زلزالي (NM) يمكنه بنجاح اكتشاف العديد من إشارات التصدع الضعيفة الناجمة عن حركة الانزلاقات الأرضية، والصحة الهيكلية، والتصدع الهيدروليكي، والمعالم التآكلية، وآليات تخفيف الإجهاد.